MINISTRY OF EDUCATION AND TRAINING

VIETNAM NATIONAL CHEMICAL GROUP

VIET NAM INSTITUTE OF INDUSTRIAL CHEMISTRY

Summary of

DOCTORAL THESIS IN CHEMISTRY

Major: Theoretical and Physical Chemistry

Code: 9.44.01.19

RESEARCH ON SYNTHESIS AND MODIFICATION OF ETHANOL ELECTROOXIDATION CATALYSTS Pt/rGO AND Pd/rGO, APPLY ON THE PREPARATION OF CATALYST INKS FOR THE ANODE IN DEFC

NGUYỄN MINH ĐĂNG

Supervisor

1. **Prof. Dr. VU Thi Thu Ha**
2. **Prof. Dr. LE Quoc Hung**

HA NOI - 2021

A- GENERAL INTRODUCTION

1. The urgency of the thesis

Nowadays, direct-ethanol fuel cell – DEFC is an electric device in which ethanol is fed directly. Moreover, ethanol has less toxic and can be obtained in great quantity from biomass through a fermentation process from renewable resources. However, catalysts in DEFC face significant challenges like working in low temperatures, activity in breaking C-C bond, and poisoning by CO-like intermediates

In recent years, numerous articles that studied electrocatalysts based on Pt, Pd, and supported on graphene in ethanol electrooxidation were published. The papers reported about modified catalysts by mono-, bi- or tri-metal or metal oxide such as Sn, Ru, Ni, Co, CeO, CuO, etc.

Since 2012, National Key Laboratory for Petrochemical and Refinery Technology – KEYLAB PRT conducted by Prof. Vu Thi Thu Ha has researched graphene material and Pt/rGO-based catalysts in alcohol electrooxidation. Recently, KEYLAB PRT has been published a number of articles in ISI or national chemistry journals. Involve in the direction in the research of KEYLABPRT, the thesis is chosen the title "**Research on synthesis and modification of ethanol electrooxidation catalysts Pt/rGO and Pd/rGO, apply on the preparation of catalyst ink for the anode in DEFC**".

The thesis is carried out under the scientific guidance of Prof. Dr. Vu Thi Thu Ha and Prof.Dr. Le Quoc Hung.

2. The aims and the main contents of the thesis

The aim of the thesis is "Research, synthesis, and modification of ethanol electrooxidation catalysts Pt/rGO and Pd/rGO, apply in the preparation of anodic catalyst inks in direct ethanol fuel cell (DEFC)".

The main contents of the thesis are:

- Research on the synthesis and characteristic properties of graphene oxide support;
- Research on synthesis and modification of ethanol electrooxidation catalyst Pt/rGO and Pd/rGO, by Al-Si

promoter.

- Research on preparation and characteristic properties of anodic catalyst inks; the influence of the components in the inks on catalytic activities, catalyst layer properties of the anode in DEFC.

3. Scientific and practical meanings of the thesis

About scientific meanings, the thesis has some contributions to studying electrocatalyst based on noble metal (Pt, Pd) on graphene in ethanol oxidation and preparing catalyst inks, the anode in a direct ethanol fuel cell. Accordingly, it may be an effective reference in science.

About practical meaning, the thesis will result in increasing efficiency of Pt- and Pd-based electrocatalysts in ethanol oxidation. Hence, preparation and application DEFC in life will become easy and more possibilities in the future.

4. The new contributions of the thesis

- ✓ The modified Pd/rGO catalyst by an Al-Si-Na promoter (Pd-Al-Si-Na/rGO) has been successfully synthesized, which has a high activity for the ethanol electrooxidation in an alkaline medium with I_F of 16138 mA mg_{Pd}^{-1}. The data is higher than the published ones of the based-on Pd catalyst. The role of Na in increasing the activity durability and anti-poisoning ability of the modified Pd/rGO catalyst was clarified (the I_F value, after 500 cyclic voltammetry cycles, decreased by about 32%), due to the formation of the $NaPd_3O_4$ cubic phase, which has high activity and durability, leads to increased bonding between Pd and rGO support;
- ✓ Ethanol was identified as the most suitable solvent in studied ones (water, n-butylacetate, isopropanol, and ethanol) for preparation of the CI-Pt-Al/rGO catalyst ink, coated on the anode of DEFC, allowing the catalyst to show the highest activity in the ethanol electrooxidation, in both acidic medium (I_F is 1456 mA mg_{Pt}^{-1}) and alkaline (I_F is 1793 mA mg_{Pt}^{-1}). No cracks on the surface of the electrodes were observed aftercoating the ink. The maximum power density of the direct ethanol fuel cell with the proton exchange membrane) or anion

exchange membrane (AEM-DEFC), using the anode reached the highest value, 19.10 mW cm^{-2} and 27.07 mW cm^{-2}, respectively;

- ✓ The anode coated CI-Pd-Al-Si-Na/rGO catalyst ink, for the anode of AEM-DEFC was fabricated. No cracks on the surface of the electrodes were observed after coating the ink. The maximum power density of the DEFC is 43.0 mW cm^{-2}. The energy conversion efficiency reached 7.83% after more than 7 hours of work with stable potential at about 0.5 to 0.6 V, higher than the published studies on AEM-DEFC with based-Pd catalysts.

5. The structure of the thesis

The thesis has 136 pages, contains 12 tables, 66 figures, and diagrams, which was divided into parts following: Abstract (2 pages), Chapter 1 Literature review (46 pages), Chapter 2 Experiments and Methodologies (17 pages), Chapter 3 Results and Discussion (48 pages), Conclusion (2 pages), New contributions of the thesis (1 page), List of published articles (2 pages) and References (16 pages and 143 references).

***

B – THE MAIN CONTENTS OF THE THESIS

Chapter 1: LITERATURE REVIEW

Ethanol is a renewable fuel with a number of benefits like less toxic, environmentally friendly, and high availability from biomass. Direct ethanol fuel cells (DEFC) convert the chemical energy of ethanol without reforming step or pretreatment directly into electrical energy. DEFC has attracted much attention recently in the search for alternative energy resources. However, its energy efficiency is lower than the direct methanol fuel cell or hydrogen fuel cell, the value is less than 10 %. DEFC are developed both in acidic media based on the principle of proton exchange membrane (PEM-DEFC) and in alkaline media based on that of anion exchange membrane (AEM-DEFC). The inherently faster kinetics of the oxygen reduction reaction in an alkaline fuel cell allows the use of non-noble and low-cost metal electrocatalysts such as silver and nickel, making the alkaline fuel cell a potentially low-cost

technology compared to the acidic fuel cell, which employs platinum catalysts.

A lot of papers have been addressed to ethanol electrooxidation on Pt(Pd)-based on nanocarbon material, especially graphene. However, some intermediate as acetaldehyde, CO_{ads}, CHO_{ads} are poisonous impacts for catalysts based on noble metal. As a result, the researcher focus on modified material that has high activity and stability in ethanol electrooxidation. Hence, the catalyst has been modified by mono-, di- or tri-metal promoter as Sn, Ru, Co, Ni, etc or metal oxide like CeO, CuO, etc.

Catalyst ink preparation also has much attractive attention to researchers. Almost studies concentrated on the impacts of solvent, nafion per catalyst ratio, or combination to both characteristics properties of the catalyst layer and electrode operation.

In Vietnam, several research groups synthesized catalysts based on Pt on nanocarbon materials and they have gotten some good talents. Especially, KEYLAB PRT led by Prof. Vu Thi Thu Ha has numerous published articles on ISI journal and scientific project, which report about modified Pt-, Pd-based catalysts on graphene support. The materials have superior activity and stability in both ethanol and methanol electrooxidation. Besides, DEFC modeling with high power density and efficiency was prepared.

Chapter 2: METHODOLOGIES

2.1. Chemicals and equipment

Chemicals have origin from Sigma Aldrich, Merck, Fuelcell Store (USA), and Vietnam. Several specific types of equipment used were in the thesis as ultrasonic homogenizer, centrifuge filter, spin coater.

2.2. Method of synthesis

2.2.1. Preparation of graphene oxide

GO slurry was prepared by the modified Hummers' method, which was followed by researched results from KEYLAB PRT.

2.2.2. Preparation of PtAG catalyst

Pt-Al/rGO (PtAG) catalyst was prepared by wet immigration from Al-isopropoxide, GO slurry, $H_2PtCl_6.6H_2O$ and ethylene

glycol (EG) reducing agent. The reaction was stirred in 24 hours at 110^{o}C.

2.2.3. Preparation of Pd-based on rGO modified by Al-Si-Na promoters

Based-Pd/rGO catalyst modified by Al-Si-Na was made from $PdCl_2$, GO slurry, Al-isopropoxide, tetra-ethyl ortho-silicate (TEOS), and CH_3COONa. We used two reducing agents with respective conditions: stirred at 110^{o}C for 24 hours with EG, and stirred at 25^{o}C for 15 hours with $NaBH_4$.

2.2.4. Preparation of catalyst inks

Catalyst inks are a combination of catalyst slurry, solvent, and nafion solution. The components are homogenized by ultrasonic waves. The solvents were investigated like n-butyl acetate (NBA), isopropyl alcohol (IPA) and ethanol (EtOH).

2.3. Coating catalyst inks, anode preparation, and DEFC assembly

2.3.1. Coating catalyst inks and anode preparation

Catalyst inks were coated on carbon cloth by spin coating. The electrode area was of 10 cm^2 with a mass density of 2.5 $mg.cm^{-2}$ (follow by the catalyst).

2.3.2. Pretreatment of ion exchange membrane

The nafion membrane was pretreated in H_2SO_4 1 M while the anion exchange membrane was bathed in NaOH 1M. Both pretreatments have occurred at their own boiling temperature.

2.3.3. Membrane electrode assemblies preparation

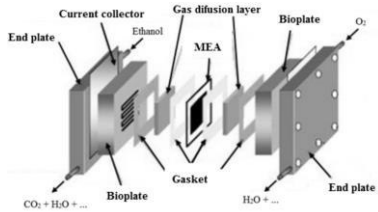

Figure 2.1. Structure of DEFC

Membrane electrode assemblies (MEA) was prepared by a hot press method under the pressure of 5 Mpa at 135^{o}C for 3 minutes. The cathode is a Pt black on carbon cloth (density of 2 $mg.cm^{-2}$). DEFC contains parts introduced as a structure

in Figure 2.1. Some bolts keep all as a block.

2.4. Methods to investigate characteristic physicochemical properties

Characteristic properties of the catalyst were investigated by physicochemical methods like XRD, FT-IR, SEM, TEM, XPS, ICP-OES, EDX, and Raman.

2.5. Measurement of electro activities of catalysts

Electrochemical tests were addressed at room temperature on a PGS-ioc-HH12 Potentiostat/Galvanostat with a 3-electrode system in KEYLAB PRT. The working electrode that is a glassy carbon with a diameter of 5 mm was coated an amount of 10 µL catalyst slurry with nafion. Catalyst inks were coated directly on the surface of the electrode.

Electrochemical activities of catalysts in ethanol oxidation were determined by the cyclic voltammetry (CV) method with a scan rate of 50 mV.s-1. In an acidic (H_2SO_4) media, the range of potential was from 0 to 1 V, and in an alkaline (NaOH) media, it was from -0.8 to 0.5 V. The solution was saturated by nitrogen before every measurement.

The chronoamperometry method was trialed in alkaline media at a constant potential of -0.25 V.

2.6. Determine power density and energy efficiency of DEFC

The power density of DEFC was addressed by the polarization method on a singe cell at a temperature of 50°C. In the anode, a solution of ethanol 2 M was fed with PEM-DEFC while a solution of ethanol 2 M and NaOH 1 M was injected, the flowrate was 10 mL.min-1. In cathode, a flow of humidified oxygen was used as a fuel.

The energy efficiency of DEFC was determined at 25°C by a formula following:

$$\varepsilon = \frac{I \int_{t_0}^{t_t} V dt}{\Delta H^0_{complete}} \frac{1}{M^F_{TOT}} \qquad (1)$$

Where: ε: efficiency, %; I = 300 mA: current density; V(t).dt: a function of potential of the cell over time t, V.s: testing time, s;

$\Delta H^0_{complete} = -1326\ \ kJ\ \ mol^{-1}$: enthalpy of completed ethanol oxidation; M^F_{TOT}: total molar of ethanol that has been converted, determined on chromatography with a thermal conductivity detector.

Chapter 3: RESULTS AND DICUSSION

3.1. Synthesis and characteristic properties of graphene oxide

Observe a change specific peak on XRD patterns (see Figure 3.1), from 2θ ≈ 26° to 2θ ≈ 11°, that is corresponding to the spacing between diffracting planes was widened from 4 Å in graphite to 8 Å in graphene oxide structure.

Raman spectra of GO (see Figure 3.2) introduced peaks of the D or G band at 1350 cm^{-1} và 1575 cm^{-1}, respectively. The intensity ratio between D/G bands equal to 0.6, corresponding to the Raman spectra of GO following published papers.

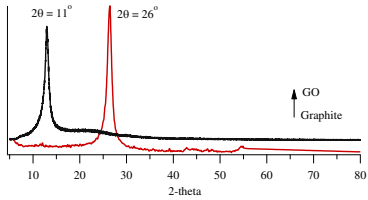

Figure 3.1. XRD patterns of GO

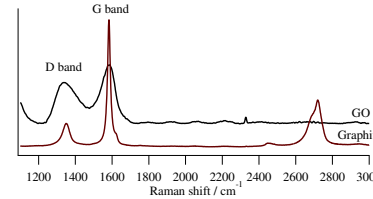

Figure 3.2. Raman spectra of GO

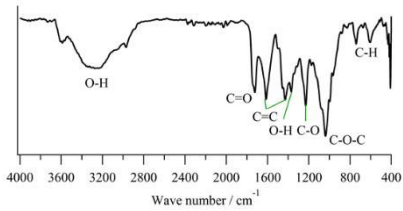

Figure 3.3. FT-IR spectra of GO

Figure 3.3 showed that characteristic vibration bands of O-H (3000 to 3500 cm^{-1} and 1429 cm^{-1}), C=O (1722 cm^{-1}), C=C (from 1400 to 1600 cm^{-1}) C-O, O-C-O (from 100 to 1200 cm^{-1}) and C-H bonding (from 600 to 800 cm^{-1}).

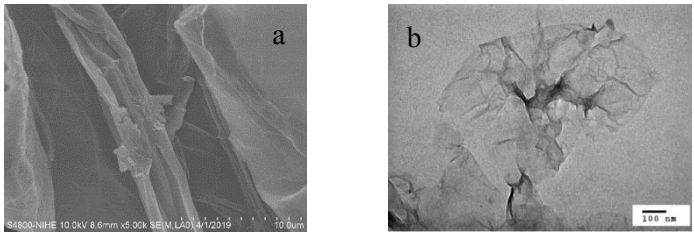

Figure 3.4. SEM (a) and TEM (b) image of GO

Figure 3.4 presented SEM and TEM images of GO, which has a few layers with a size from 2 to 4 µm and see-though. Moreover, some creases were observed on the layer.

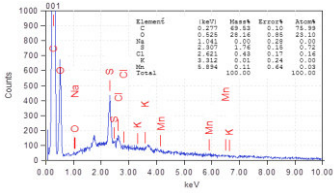

Figure 3.5. EDX spectra of GO

The EDX spectra of GO in Figure 3.5 showed that C and O have a high concentration in the structure of GO. Its C/O ratio was from 2.1 to 2.9, which is a characteristic property of GO.

In conclusion, the above results prove that GO was synthesized successfully from exfoliated graphite by the modified Hummers method.

3.2. Synthesis and characteristic properties of PtAG catalyst

XRD pattern (see Figure 3.6) of rGO presented a broad diffraction peak attributed to the (002) carbon peak of rGO between 2θ from 24° to 26°. While, on that of PtAG catalyst, the typical reflection peaks at 2θ = 39°; 46° and 69°, corresponding with the characteristic Pt (111), Pt (200), and Pt (220) were observed. However, there were no peaks of Al or Al_2O_3 on the pattern since Al may be an amorphous phase.

Raman spectra in Figure 3.7 showed peaks of G band of C-C bonding in graphite and that of D band of 2D structure in graphene material. However, I_D/I_G ratios were different following an order: PtAG (1.07) < rGO (1.42). It means that there are more defects in graphene composites, cause of the presence of Pt or Al on the graphene surface.

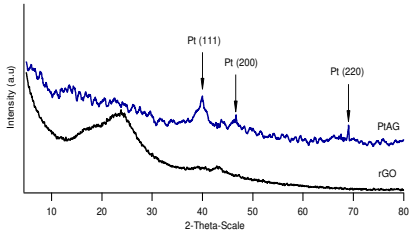

Figure 3.6. XRD patterns

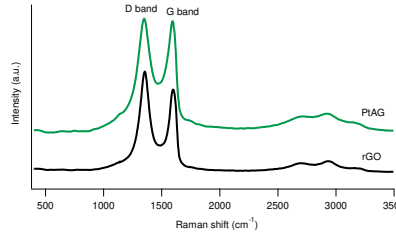

Figure 3.7. Raman spectra

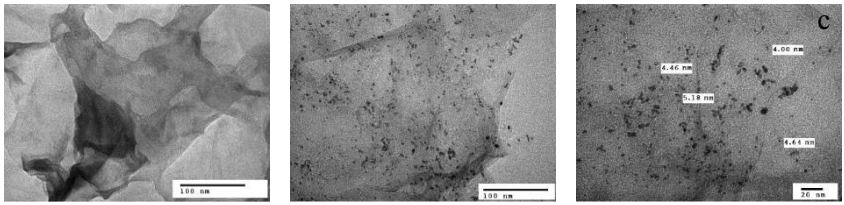

rGO PtAG catalyst

Figure 3.8. TEM image of rGO and the catalyst

TEM image of rGO and PtAG catalyst (see Figure 3.8) presented a clear multi-layer of graphene oxide that superposed on each other. Moreover, the uniform dispersion of Pt nanoparticles on graphene layers was observed. The average size of the particles was at from 4 nm to 5 nm.

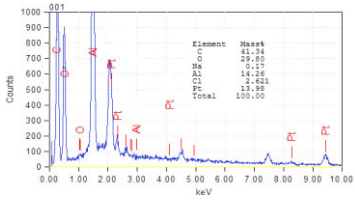

Figure 3.9. EDX spectra of the PtAG catalyst

EDX spectra of the PtAG catalyst (see Figure 3.9) showed that the mass concentration of Pt and Al were following order 13.98% and 14.26%, it means the ratio Pt/Al was approximate 1/1, which equated to 14.3% of the theoretical value.

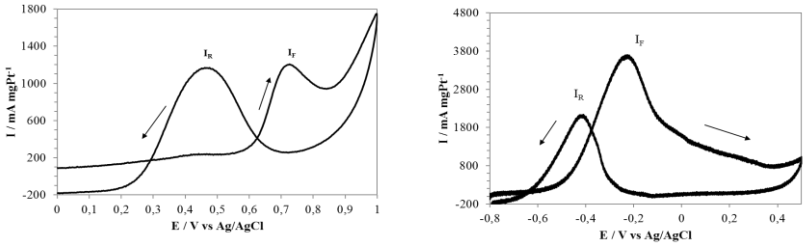

H_2SO_4 0.5 M + C_2H_5OH 1 M *NaOH 0.5 M + C_2H_5OH 1 M*

Figure 3.10. CV curves of PtAG catalyst in both of mediums

CV curve of PtAG catalyst in both medium (see Figure 3.10) presented its high activity in ethanol electrooxidation. For example, in acidic media, I_F and I_B value were at 1200 mA mg_{Pt}^{-1} and 1136 mA mg_{Pt}^{-1}, respectively, I_F/I_B = 1.03. While the peaks were at 3674 mA mg_{Pt}^{-1} and 2060 mA mg_{Pt}^{-1}, I_F/I_B = 1.78 in alkaline medium. It means that the catalytic activity of PtAG was higher in alkaline than in acidic medium.

3.3. Synthesis and characteristic properties of modified Pd/rGO

3.3.1. Research on the effect of reducing agents on properties of Pd-based/rGO catalyst

CV curve and its data of Pd-based catalysts (see Figure 3.11 and Table 3.1) presented that Al-Si modified catalysts have 45.7% and 43.5% higher than non-modified ones in both cases of reducing by EG and $NaBH_4$, respectively. In addition, when the agent $NaBH_4$ was used instead of EG, the catalyst presented more catalytic activity and resistance against the poisoning of intermediate compounds. Specifically, the catalyst reduced by $NaBH_4$ with the bimetallic Al-Si promoter phase (PASG.N) showed 1.4 times higher activity than by EG (PASG.E). In addition, after 4000 s of working, the current density of the PASG.N catalyst was 6.5 times higher than that of PASG.E (see Figure 3.12). Furthermore, both electrochemical activity and the ratio of the forward scanning peak current density to the reverse scanning peak current density, (I_F/I_B) of the PASG.N catalyst (1.93), were also higher than those of the PASG.E catalyst (1.28) were. Consequently, $NaBH_4$ could be a better agent for Pd-based catalyst reduction than EG.

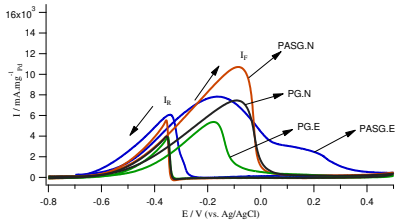

Figure 3.11. CV curve of the Pd/rGO catalyst

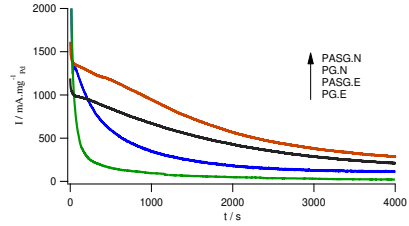

Figure 3.12. CA curve of the Pd /rGO catalyst

Table 3.1. CV peak data of modified Pd /rGO catalyst

Catalyst	I_F / mA mg^{-1}_{Pd}	I_B / mA mg^{-1}_{Pd}	I_F/I_B
PG.E	5369	3915	1.37
PASG.E	7822	6111	1.28
PG.N	7457	3967	1.88
PASG.N	10705	5531	1.94

Table 3.2. Concentration of Pd and promoter phase of the Pd/rGO catalyst

Catalyst	Theoretical mass concentration		Mass concentration following ICP-OES	
	Pd / %	Promoter phase / %	Pd / %	Promoter phase / %
PG.E	28,57	-	8,53	-
PASG.E	27,20	1,36 (Al); 3,42 (Si)	8,34	0,34 (Al); 2,15 (Si)
PG.N	28,57	-	9,71	0,15 (Na)
PASG.N	27,20	1,36 (Al); 3,42 (Si)	8,78	0,34 (Al); 2,41 (Si); 0,12 (Na)

ICP-OES results (see Table 3.2) introduced the mass concentration of Pd that was 8.34 to 9.71 % equated about one-third to the theoretical value. Moreover, the Pd loading of the catalysts reduced by $NaBH_4$, 9.71% and 8.78% in PG.N and PASG.N, are higher than that reduced by EG, 8.83% and 8.34% in PG.E and PASG.E, respectively. Another result is that the concentration of the promoter phase was determined in order 0.34 % (Al) and 2.15 to 2.41% (Si). Especially, there was the presence of Na in the catalyst

reduced by $NaBH_4$, which was at 0.12 to 0.15%. The reason may be that Na has not yet removed clearly by washing.

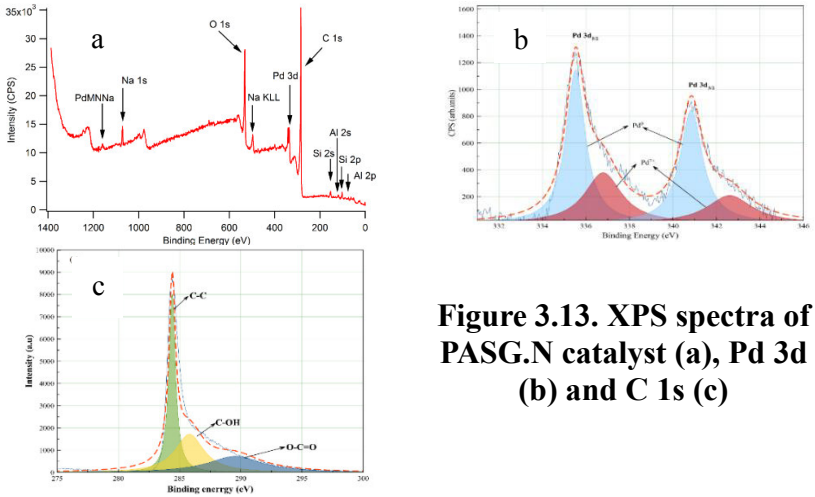

Figure 3.13. XPS spectra of PASG.N catalyst (a), Pd 3d (b) and C 1s (c)

XPS spectra of the PASG.N catalyst (see Figure 3.13a) showed that the Al and Si compounds obtained in the catalysts exist as pseudo-boehmite (Al-OOH) and amorphous silica (SiO_2). In addition, a characteristic peak of Pd 3d was also observed on the spectrum. Especially, the random appearance of Na 1s and Na_{KLL} that corresponds with the above ICP result.

Figure 3.13b showed the Pd 3d core-level XPS spectrum of PASG.N catalyst which is resolved into $3d_{5/2}$ and $3d_{3/2}$ doublets caused by spin-orbital coupling The Pd 3d signals for catalysts can be deconvoluted into two pairs of doublets, which can be attributed to metallic Pd (0) and Pd (II). The metallic Pd phase was proved to be the major contribution as the intensities of Pd (II) were quite lower than those of Pd (0). It means that reducing from Pd (II) to Pd (0) reaction has happened successfully

Besides, the relative signal intensities of Pd (0) and Pd (II) of PASG.N catalyst were different, 53.56% and 37.81%, respectively. In addition, the Pd weight density on the catalyst surface was 8.23%, while that of Al, Si, and Na was 2.38%, 3.44%, and 2.19%, respectively, which are similar to ICP results. Moreover, the ratio between Pd (0) and Pd (II) PASG.N in XPS result of PASG.N,

approximately 1.41, is higher than that of PASG.E, approximately 1.01.

In figure 3.13c, after the deconvolution, two major peaks were identified and assigned as sp^2 C=C at 284.4 eV (due to the graphitic carbon), sp3 C-O at 285.8 eV and 289.4 eV (due to the hydroxyl and epoxy groups with graphene framework).

3.3.2. Research on the effect of Na promoter on properties of Pd-based/rGO catalyst

It is obvious that whatever reducing agents were used during synthesis (EG or NaBH4), all Na-doped catalysts showed significantly higher electrocatalytic activity compared with the non-Na-doped catalysts (see Figure 3.14 and Table 3.3).

Therefore, the role of the promoter of Na was completely independent of the effect of the reducing agent on the electrooxidation of ethanol. For instance, the I_F value of PASGN.N was at 16138 mA mg^{-1}_{Pd}, which is the most superior electrochemical activity (I_F = 16138 mA mg^{-1}_{Pd}) compared to published articles about Pd-base catalyst. Furthermore, the I_F/I_R ratio of the Na-doped catalyst reduced by $NaBH_4$ has a better value than reduced by EG. It means that ethanol electrooxidation in alkaline media with PASGN.N occurs more completely.

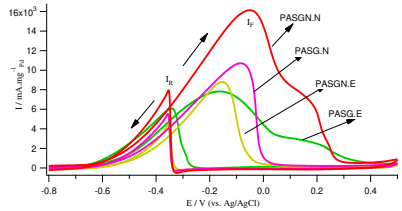

Figure 3.14. CV curve of the Pd/rGO catalyst

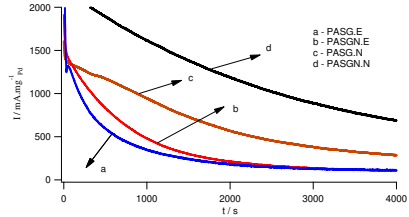

Figure 3.15. CA curve of the Pd/rGO catalyst

Table 3.3. CV data of the Pd/rGO catalyst modified by Al-Si (Na)

Xúc tác	I_F , mA mg^{-1}_{Pd}	I_B , mA mg^{-1}_{Pd}	I_F/I_R
PG.E	5369	3915	1,37
PNG.E	6988	5273	1,33
PASG.E	7822	6111	1,28
PASGN.E	8800	4367	2,02

PG.N	7457	3967	1,88
PNG.N	8357	4687	1,78
PASG.N	10705	5531	1,94
PASGN.N	16138	7949	2,03

Besides, CA curves (see Figure 3.15) proved that Na presence assisted the Pd-base catalysts in enhancing the resistance against poisoning of intermediate compounds in ethanol electrooxidation in alkaline media. Na presence may cause increasing adsorption of oxygen and fuel on the surface of the catalyst, which brings out an increase of catalytic activity.

Results in Table 3.4 showed that the fraction of elements in modified Pd/rGO catalysts equals about 1/3 to theoretical concentration. Moreover, Pd concentration in the catalyst reduced by $NaBH_4$ was higher than that reduced by EG.

Table 3.4. Mass concentration of Pd and promoter phase in Pd-based/rGO

Catalyst	Theoretical mass concentration		Mass concentration following ICP-OES	
	Pd / %	**Promoter phase / %**	**Pd / %**	**Promoter phase / %**
PNG.E	26.40	7.61 (Na)	7.51	2.52 (Na)
PASGN.E	25.23	7.25 (Na); 1.26 (Al); 3.15 (Si)	7.57	2.40 (Na); 0.27 (Al); 2.30 (Si)
PNG.N	26.40	7.61 (Na)	9.21	2.72 (Na)
PASGN.N	25.23	7.25 (Na); 1.26 (Al); 3.15 (Si)	8.54	2.62 (Na); 0.29 (Al); 1.83 (Si)

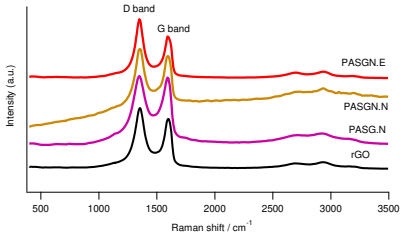

Figure 3.16. Raman spectra of rGO and catalysts

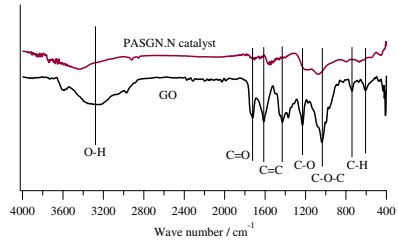

Figure 3.17. FTIR spectra of GO and catalyst

Raman spectra of catalysts (see Figure 3.16) presented that the peak intensities of the G band (I_G) at 1600 cm^{-1} corresponding to the sp^2 - hybrid carbon state in the hexagonal lattice of graphite and the D band (I_D) at 1350 cm^{-1} being characteristic for the vibration of sp^3 - hybrid C in the disorder structure of graphene sheets. The Raman spectra of catalysts were also similar to those of rGO, but the intensity of the I_D/I_G ratio of catalyst increased in the following order: PASG.N (1.02) < PASGN.N (1.10) < rGO (1.42) < PASG.E (1.98).

In the infrared spectra (see Figure 3.17) in that of the PASGN.N catalyst, some specific peaks of GO were reduced clearly. Moreover, the presence of a C=C bond near 1600 cm^{-1} was found out in the catalyst. Consequently, the reduction of GO was successful.

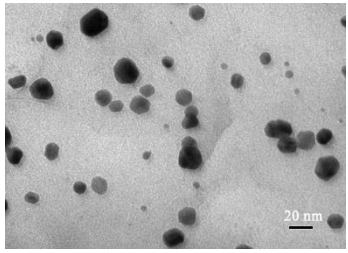

PASG.E

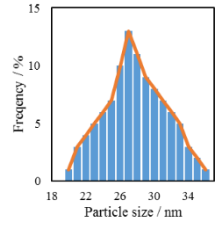

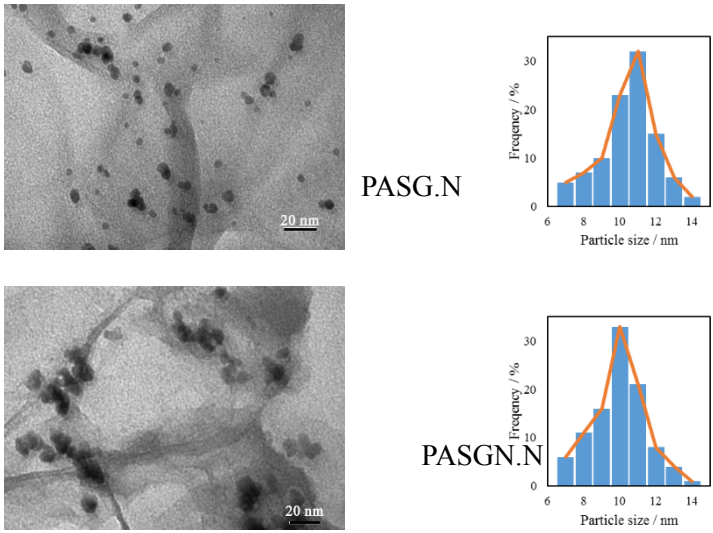

Figure 3.18. TEM image and size distribution of catalysts

The TEM image of catalysts (see Figure 3.18) showed that a less uniform and sparse dispersion of metallic nanoparticles is described for the catalysts. For example, the PASG.N and PASGN.N catalysts (reduced by $NaBH_4$) have their activity particle size from 7 nm to 14 nm, while that of PASG.E catalyst (reduced by ethylene glycol) was three times larger, about 20 nm to 36 nm. It means that reducing agent $NaBH_4$ is improving the size of the catalytic active phase particle. Furthermore, TEM images of the PASGN.N (Na-doped) and PASG.N (non-Na-doped) catalyst introduced that Na-doped significantly enhanced the dispersion of metallic nanoparticles on the graphene support surface. The active nanoparticles of PASGN.N catalysts expanded with a higher density than those of the PASG.N catalyst, which explained the increase in the number of active sites on the surface of graphene support, considerably enhancing the catalytic activity of electrooxidation of ethanol. Moreover, the metal nanoparticles in the PASGN.N catalyst tend to aggregate from 2 to 3 particles to form larger ones at the edges of graphene sheets.

In fact, EASA of catalysts were in descending order as follows (see Table 3.5): PASG.E <PASG.N <PASGN.N. This affection is similar to the TEM image described above. The particle size is higher and the activity surface is lower.

Table 3.5. EASA results and average particle size of catalysts

Catalysts	Average particle size / nm	Q / mC	EASA / $cm^2\ mg^{-1}_{Pd}$
PASG.E	28,07	$1,902 \times 10^{-3}$	1502
PASG.N	10,49	$2,583 \times 10^{-3}$	1937
PASGN.N	9,97	$2,693 \times 10^{-3}$	2076

On the other hand, the Na addition also improved the stability of the Pb-based catalyst in ethanol electrooxidation (see Figure 3.19 and Table 3.6).

Table 3.6. I_F of catalyst after 500 CV scaning cycles

Catalyst	Forward current density - I_F / mA mg^{-1}_{Pd}							
	I_F 15th	I_F 100th	I_F 200th	I_F 200th/ I_F 15th	I_F 300th	I_F 400th	I_F 500th	I_F 500th/ I_F 15th
PASGN.N	16138	14175	13816	0,84	12751	12342	10864	0,68
PASG.N	10705	9100	8565	0,80	6884	4956	2884	0,27

In the case of the PASGN.N catalyst, the electrochemical activity of the catalysts decreased quite slowly after 200 cycles, where I_F 200th was equal to 84% of the reference (I_F 15th). The slow reactivity holds up to 500 cycles, where the forward current density value I_F 500th was equal to 68% of the reference.

In the case of the PASG.N catalyst, the activity has a similar behavior. However, the rate of its decrease was faster than that of PASGN.N, corresponding to the 500th current density remained 27% of the reference.

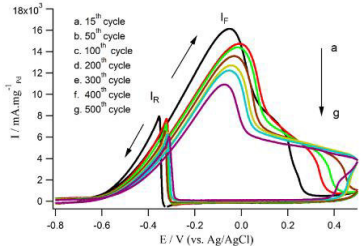

Figure 3.19. CV curve of PASGN.N catalyst

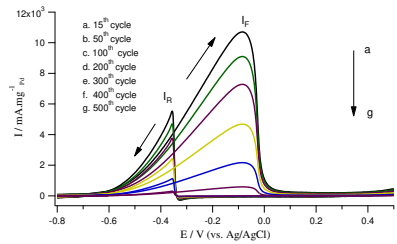

Figure 3.20. CV curve of PASG.N catalyst

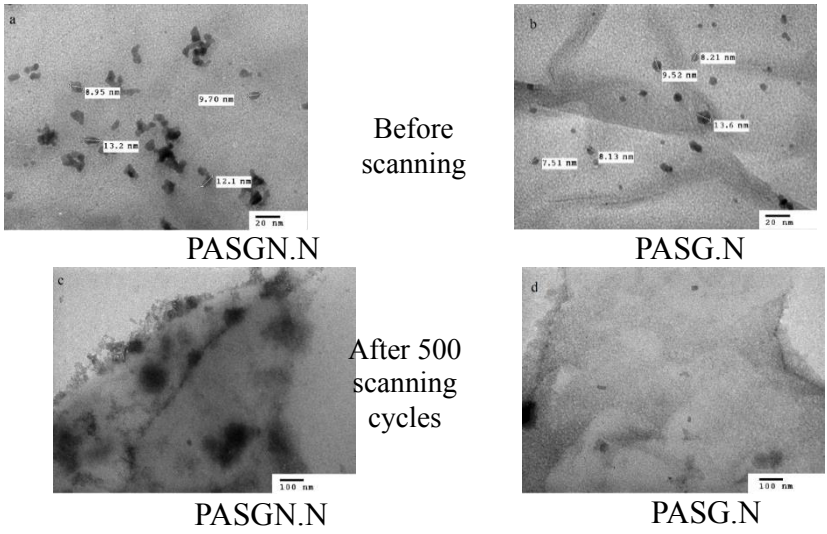

Figure 3.21. TEM image of catalysts

Besides, the combination between active phase (Pd nanoparticles) and support, graphene can become more sustainable under the presence of Al-Si-Na addition, which is observed on TEM images of the catalysts after 500 scanning cycles (see Figure 3.20). For instance, in the case of the PASGN.N, the metal particles tend to aggregate into clusters of very large size, from 60 nm to 130 nm, which dispersed in separate zones. The density of metallic nanoparticles on the graphene surface is considerably reduced while that at the edges of graphene sheets tends to increase. However, in the case of the PASG.N catalyst, almost no metallic particles are presented on the surface of the graphene after 500 scanning cycles. This result is in accordance with the catalytic deactivation after 500 scanning cycles as described previously. The reason may be the cubic phase of $NaPd_3O_4$ was formed, led the bond between Pd and rGO to become stronger. As a result, the activity and stability of the catalyst were increased.

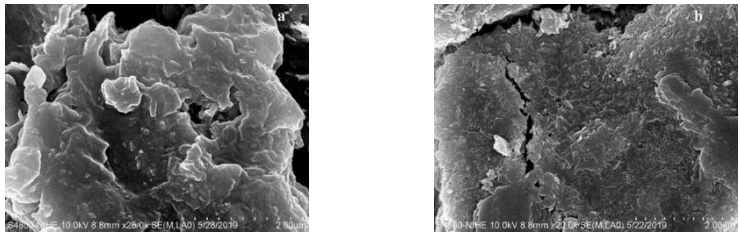

Before scanning After 500 scanning cycles

Figure 3.22. SEM image of PASGN.N catalysts

The SEM image of the PASGN.N catalyst before and after 500 scanning cycles were observed in Figure 3.21. The result showed that the catalyst looked like a homogeneous "block". However, it was broken into pieces after the reaction. Moreover, Figure 3.21(b) also showed the number of particles with columnar shape. It seems that the active phase Pd may be separated from the support and may agglomerate after hundreds of cycles. As a result, the catalytic activity was reduced.

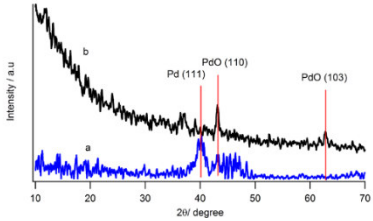

Figure 3.23. XRD patterns of PASGN.N catalyst (a) before and (b) after 500 scaning cycles

The peak at 2θ value of 40.1° corresponding to the planes Pd (111) as shown in the pattern of the catalyst before the reaction while two peaks of planes PdO (110) and PdO (103) were introduced in the catalyst after the reaction (see Figure 3.22). Consequently, the PdO crystal phase is forming during the reaction.

3.4. Fabrication and characterization of the PtAG catalyst inks for the anode in DEFC

The thesis presents the results of researches on the effects of n-butyl acetate, isopropanol, and ethanol solvents on the properties and electroactivity of catalyst ink based on Pt-Al/rGO.

Some physical properties of solvents was presented in Table 3.7.

Table 3.7. Some physical properties of solvents

Solvent	Boiling point / ºC at 760 mmHg	Độ nhớt ở 25ºC, cP	Solubility in water / g in 100 mL (20°C)
Water	100,2	0,56	-
n-Butyl acetate	126,1	0,68	0,68
Isopropanol	82,6	1,96	Miscible
Ethanol	78,2	1,07	Miscible

3.4.1. Characterization of the PtAG inks and the anode electrode

TEM images of PtAG catalyst inks (see Figure 3.24) indicate uniform distribution of Pt nanoparticles on rGO.

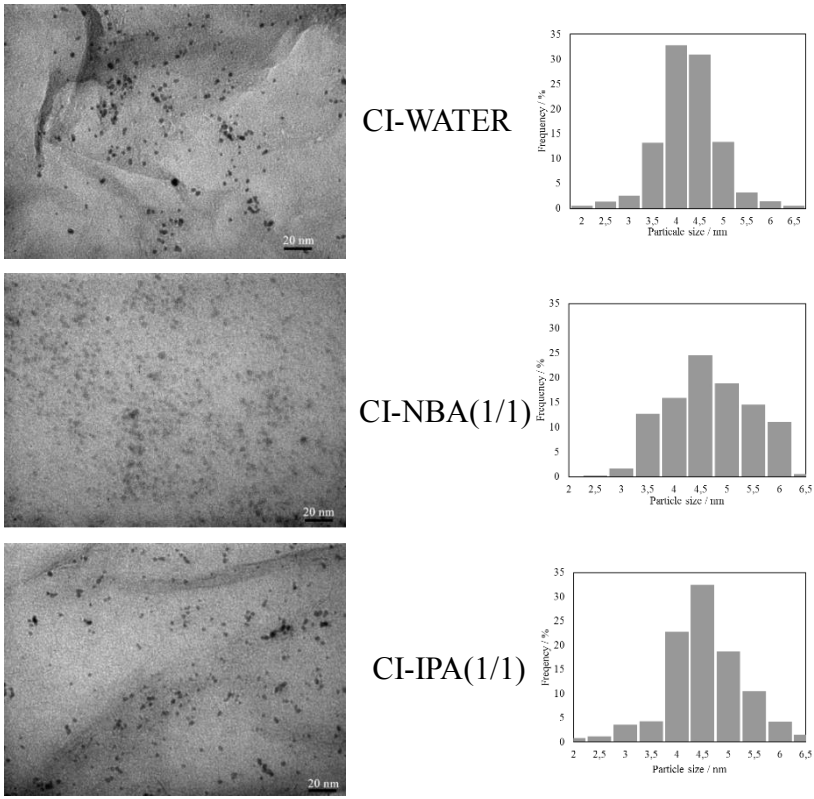

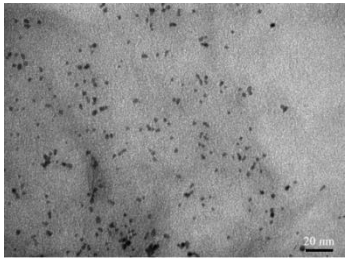

CI-EtOH(1/1)

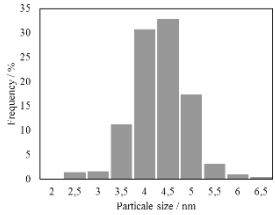

Figure 3.24. TEM image and size distribution of catalyst inks

The Pt particle size in CI-WATER ink and CI-EtOH(1/1) ink was approximately 4.0 nm. For CI-NBA(1/1) ink and CI-IPA(1/1) ink samples, there was a slight increase in the Pt particle size (4.5 nm), which can be because of the redeposition of the dissociated Pt ions from the Pt particles during ink preparation, using NBA and IPA solvents.

Figure 3.25a shows the smooth surface of the substance. Meanwhile, the surface of the CI-WATER catalyst layer has a few cracks as observed in Figure 3.25b. A carbon foam layer would be seen in Figure 6a. Figure 6b shows SEM image of the CI-WATER catalyst layer with the I-shape cracks and pinholes that due to the low interaction between ionomers and the PtAl/rGO catalyst.

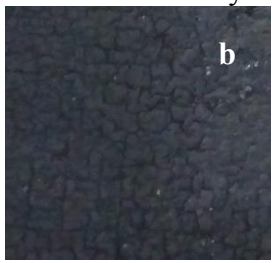

Figure 3.25. Photographs of the surface of the carbon cloth substance (a), and the CI-WATER ink-coated electrode (b)

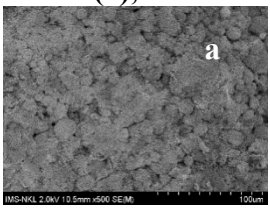

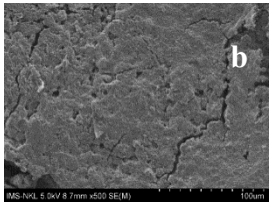

Figure 3.26. SEM images of the carbon cloth substance (a), and the CI-WATER ink-coated electrode (b)

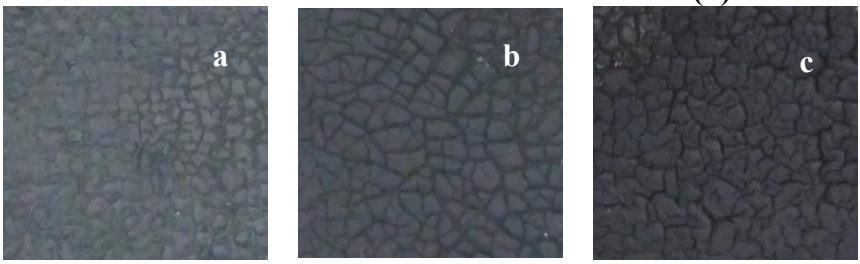

Figure 3.27. Photographs of the surface of the electrode-coated CI-NBA(1/1) (a), CI-NBA(1/0.5) (b), and CI-NBA(1/2) inks (c)

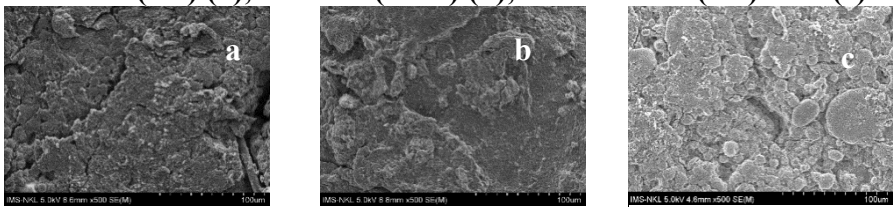

Figure 3.28. SEM images of the electrode-coated CI-NBA(1/1) (a), CI-NBA(1/0.5) (b), and CI-NBA(1/2) ink (c)

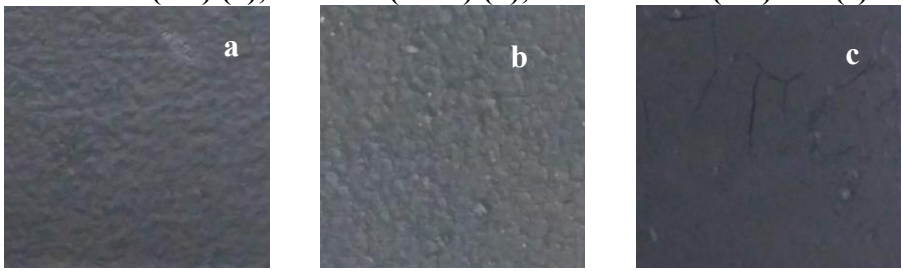

Figure 3.29. Photographs of the surface of the electrode-coated CI-IPA(1/1) (a), CI-IPA(1/0,5) (b) và CI-IPA(1/2) inks (c)

Figure 3.27 introduces the CI-NBA catalyst layers including many cracks with different shapes. SEM images of the electrode-coated CI-NBA inks showed that the surface is not smooth; the catalyst layer had an uneven density (see Figure 3.28)

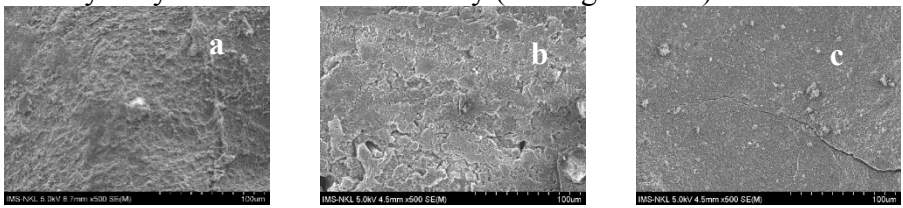

Figure 3.30. SEM images of the electrode-coated CI-IPA(1/1) (a), CI-IPA(1/0,5) (b) và CI-IPA (1/2) (c) inks

The photographs of the surface of CI-IPA ink-coated electrodes in Figure 3.29 showed that their surface was smoother than CI-NBA and CI-WATER catalyst layers. SEM images resulted that the surface of the CI-IPA(1/1) layer was the smoothest surface and there was no crack present (see Figure 30a). Thus, for CI-IPA inks, the volumic ratio between the catalyst slurry and the solvent of 1:1 (CI-IPA(1/1) ink) is the most appropriate ratio to obtain a coated electrode with uniform surface without cracks.

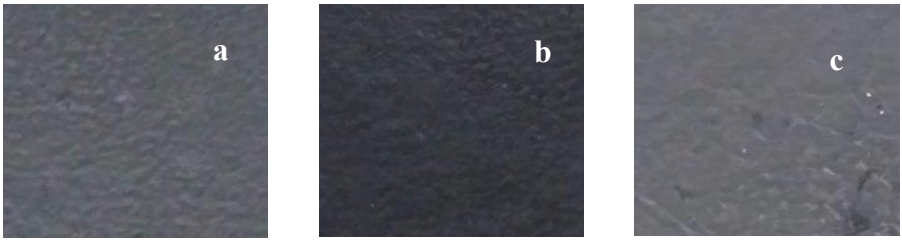

Figure 3.31. Photographs of the surface of the electrode-coated CI-EtOH(1/1) (a), CI-EtOH(1/0,5) (b), CI-EtOH(1/2) inks (c)

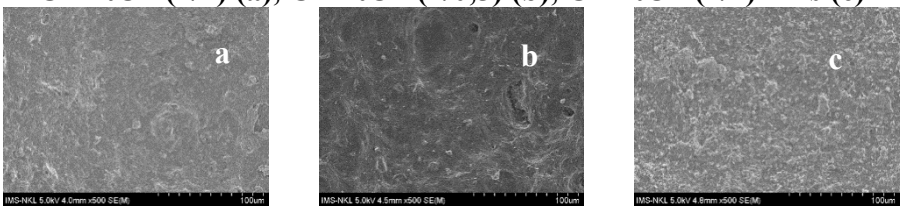

Figure 3.32. SEM images of the electrode-coated CI-EtOH(1/1) (a), CI-EtOH(1/0,5) (b) and CI-EtOH(1/2) inks (c)

The photographs and SEM images of the electrode-coated CI-EtOH inks (see Figure 3.31 and Figure 3.32) showed that their surface was smoother than that of CI-NBA, CI-WATER, and CI-IPA catalyst layers. Compared with the CI-IPA(1/1) electrode, the surface of the CI-EtOH(1/1) electrode was much flatter, smoother, and more uniform.

The above discussions were confirmed in SEM images with a larger magnification (1:50.000) (see Figure 3.33).

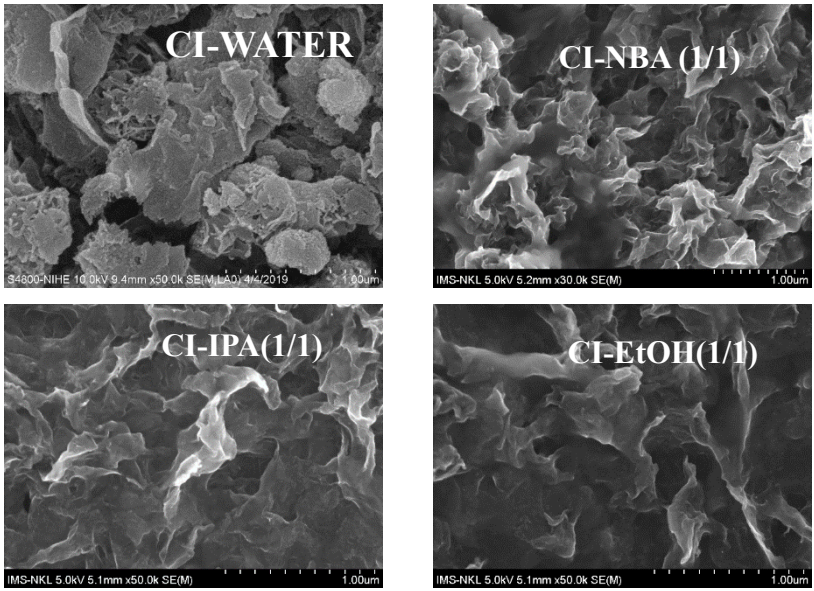

Figure 3.33. SEM images of electrode-coated inks at a magnification of 1:50.000

3.4.2. Electrochemical measurement

The activity of catalyst inks with different solvents was through the CV curve of ethanol electrooxidation in acidic and alkaline medium.

In the first place, the electroactivity of all catalyst inks in alkaline media seems to be higher than in acidic media, which is quite similar to some published articles about DEFCs.

In the second place, the electroactivity of CI-NBA inks was lower than CI-WATER (see Figure 3.34) in both media.

In the third place, the electroactivity of CI-IPA inks would be improved. The results were explained by the elimination of Nafion in an inhomogeneous microstructure of CI-IPA layers, which were introduced above, because of the reducing proton conductivity in the catalyst layer during the reaction.

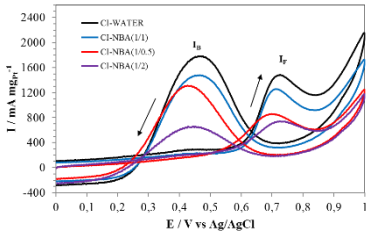

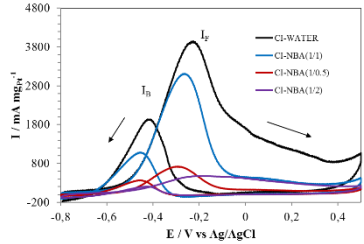

C_2H_5OH 1 M + H_2SO_4 0,5 M ***C_2H_5OH 1 M + NaOH 0,5 M***

Figure 3.34. CV curves of CI-NBA inks in the ethanol electrooxidation *(scan rate of 50 mV s^{-1}, ambient temperature)*

In the second place, the electroactivity of CI-NBA inks was lower than CI-WATER (see Figure 3.34) in both media.

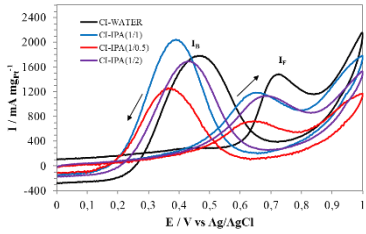

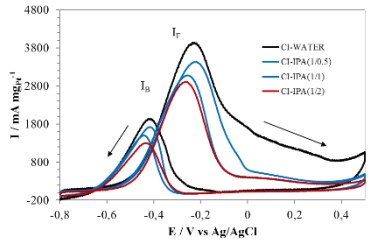

C_2H_5OH 1 M + H_2SO_4 0,5 M ***C_2H_5OH 1 M + NaOH 0,5 M***

Figure 3.35. CV curves of CI-IPA inks in the ethanol electrooxidation *(scan rate of 50 mV s^{-1}, ambient temperature)*

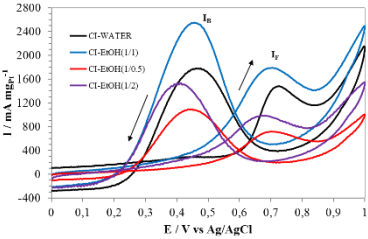

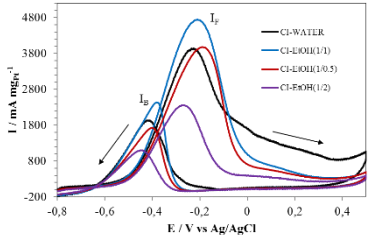

C_2H_5OH 1 M + H_2SO_4 0,5 M ***C_2H_5OH 1 M + NaOH 0,5 M***

Figure 3.36. CV curves of CI-EtOH inks in the ethanol electrooxidation *(scan rate of 50 mV s^{-1}, ambient temperature)*

A better electroactivity in the case of CI-EtOH inks was presented in Figure 3.36, especially, in the case of CI-EtOH(1/1) sample, the activity was higher than that of CI-WATER.

Table 3.8. CV data of the catalyst inks in ethanol oxidation *(scan rate of 50 mV s^{-1}, ambient temperature)*

Catalyst inks	In acidic medium			In alkaline medium		
	I_F, mA mg_{Pt}^{-1}	I_B, mA mg_{Pt}^{-1}	I_F/I_B	I_F, mA mg_{Pt}^{-1}	I_B, mA mg_{Pt}^{-1}	I_F/I_B
CI-WATER	1.486	1.784	0,83	3.951	1.894	2,09
CI-NBA(1/1)	1.257	1.478	0,85	3.114	1.182	2,63
CI-NBA(1/0,5)	857	1.310	0,65	721	364	1,98
CI-NBA(1/2)	742	661	1,12	476	220	2,17
CI-IPA(1/1)	1.187	2.046	0,58	3.435	1.724	1,99
CI-IPA(1/0,5)	723	1.261	0,57	3.080	1.496	2,06
CI-IPA(1/2)	1.133	1.693	0,67	2.911	1.298	2,24
CI-EtOH(1/1)	1.793	2.553	0,70	4.751	2.438	1,95
CI-EtOH(1/0,5)	719	1.095	0,66	3.980	1.726	2,31
CI-EtOH(1/2)	987	1.532	0,64	2.364	1.103	2,14

These results were respective to the characteristic properties of CI-EtOH inks that were introduced in the above section. It means that ethanol is the best solvent to prepare the PtAl/rGO catalyst ink, which contributes to the interaction between nafion and catalyst becoming well. Consequently, the ethanol electrooxidation would happen more easily.

3.4.3. Power density of DEFCs with electrode-coated inks

Catalyst inks were coated onto the carbon cloth to prepare anodes for DEFC.

In general, the open circuit potential of AEM-DEFCs was higher than PEM-DEFCs. According to the review of Cermenek *et al.*, this result should be explained by several advantages of AEM-DEFCs like a lower ethanol crossover, an enhancement of ethanol electrooxidation and oxygen reduction reaction kinetics, etc. compared with PEM-DEFCs.

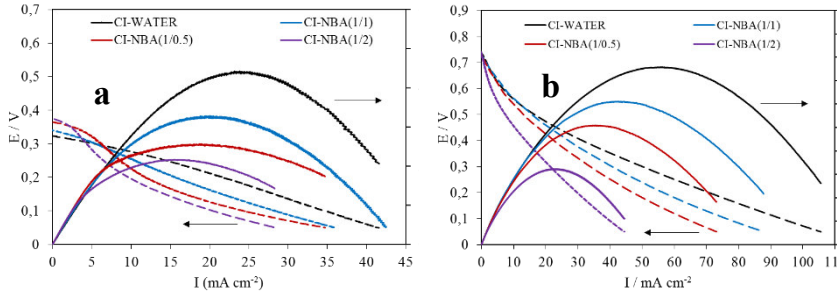

Figure 3.37. Polarization and power density curve of PEM-DEFCs (a) and AEM-DEFCs (b) using the anode-coated CI-NBA ink;

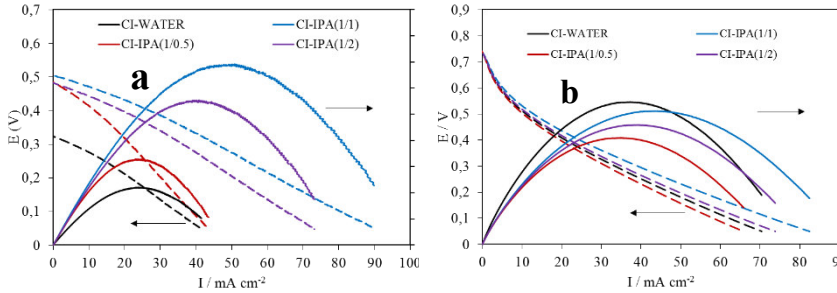

Figure 3.38. Polarization and power density curve of PEM-DEFCs (a) and AEM-DEFCs (b) using the anode-coated CI-IPA ink;

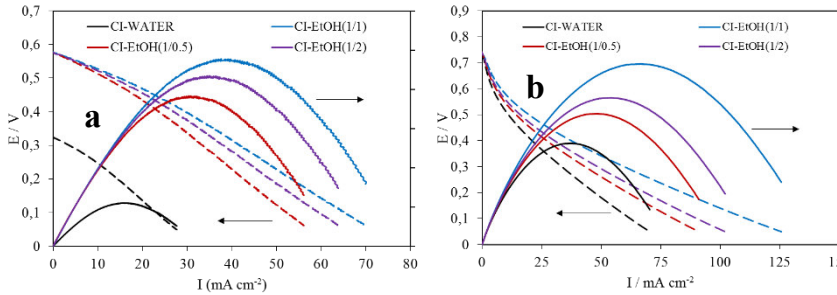

Figure 3.39. Polarization and power density curve of PEM-DEFCs (a) and AEM-DEFCs (b) using the anode-coated CI-EtOH ink;

In the case of the NBA solvent, CI-NBA anodes have a lower power density than the CI-WATER electrode (reference).

On the other hand, the IPA solvent brings out a difference. In PEM-DEFC, the power density of CI-IPA anodes was higher than the reference.

Table 3.9. Power density of DEFC with anode-coated different catalyst inks

Catalyst inks	Maximum power density, mW cm^{-2}	
	PEM-DEFC	AEM-DEFC
CI-WATER	4.42	15.17
CI-NBA(1/1)	3.29	12.23
CI-NBA(1/0.5)	2.57	10.19
CI-NBA(1/2)	2.17	6.48
CI-IPA(1/1)	13.86	14.21
CI-IPA(1/0.5)	6.60	11.35
CI-IPA(1/2)	11.09	12.72
CI-EtOH(1/1)	19.10	27.07
CI-EtOH(1/0.5)	15.29	19.61
CI-EtOH(1/2)	17.38	21.99

Besides, the polarization and power density curve of CI-EtOH anodes once again confirm that ethanol is the most suitable in the preparation of PtAl/rGO catalyst inks in DEFCs. Their power density of PEM-DEFCs was approximately 4 times higher than the reference, which was 19.10 mW cm^{-2} with CI-EtOH(1/1) anode. In the same way, in AEM-DEFCs, the power was from 1.3 to 1.8 times higher than the reference, which was 27.07 mW cm^{-2} with CI-EtOH(1/1) anode (see Table 3.9).

These results were quite corresponding to the electroactivity of all catalyst inks mentioned above.

To sum up, ethanol with the solvent ratio 1/1 not only brings out the highest electroactivity of the PtAl/rGO catalyst inks in both acidic and alkaline media but also contributes to the best power density of CI-EtOH anode in PEM-DEFCs and AEM-DEFCs.

3.5. Fabrication and characterization of the Pd/rGO ink for the anode in DEFC

TEM image results (see Figure 3.29) showed that the active particles Pd are distributed quite evenly on the thin graphene film and concentrated mainly in the outer folds or edges.

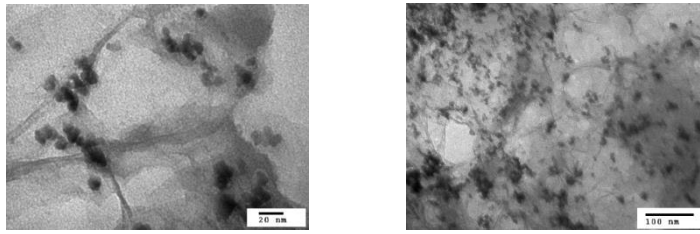

Figure 3.40. TEM image of the CI-Pd/rGO ink

Before coating Coated CI-Pd/rGO inks

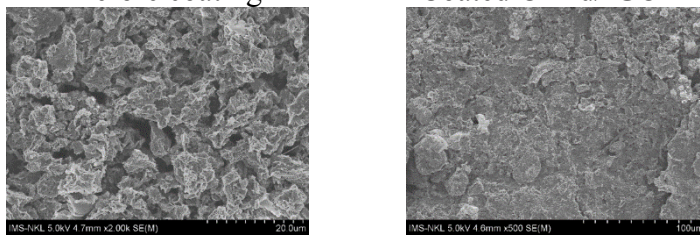

Before coating Coated CI-Pd/rGO inks

Figure 3.41. Surface images (upper) and SEM image (lower) of the anode before and after coating CI-Pd/rGO ink

Figure 3.41 showed the surface image and SEM image of the CI-Pd/rGO catalytic ink anode electrode. The catalyst layer was evenly distributed over all positions of the fabric and no cracks

appear.

The results of Figure 3.41 showed that the maximum power density of the fuel cell reaches about 43.0 mW cm^{-2} at a temperature of 50°C at a voltage of about 0.25 V.

The result of Figure 3.22 shows that the voltage of the DEFC battery decreases with time and is divided into 3 stages. In which, a stable potential range from 0.5 to 0.6 V lasts more than 7 hours.

With the obtained parameters such as I = 300 mA; integral values are determined throughout stage 2: $\int_{t_0}^{t_t} Vdt = 27687 \ \ V.s$; The total moles of ethanol reacted during this period was about 0.80 mole. Applying the formula (1) in item 2.6, the fuel cell's energy conversion efficiency is about 7.83%.

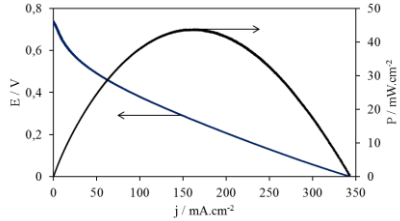

Figure 3.42. Polarization and power density curve of AEM-DEFC using CI-Pd/rGO anode

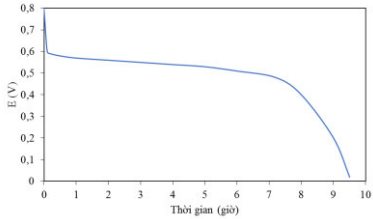

Figure 3.43. Potential of AEM-DEFC using CI-Pd/rGO anode

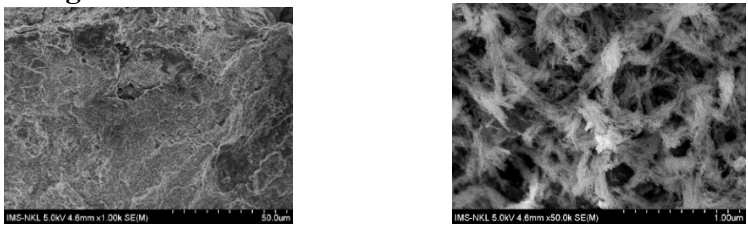

Hình 3.44. SEM image of the CI-Pd/rGO ink-coated anode after testing, at different magnifications

Figure 3.44 showed the SEM image of an anode electrode coated CI-Pd/rGO ink after the stable running process.

CONCLUSION

1. Graphene oxide was successfully synthesized by the modified Hummer method from exfoliated graphite.

2. The Pt-Al/rGO catalyst was successfully synthesized, with a metal particle size in the range of 4 to 5 nm, evenly dispersed on the graphene film. The contents of Pt and Al are respectively 13.98% and 14.26%. The Pt-Al/rGO catalyst has high electrochemical activity in the EOR reaction in both acidic and alkaline media, corresponding to the I_F current density value of 1200 mA mg_{Pt}^{-1} and 3674 mA mg_{Pt}^{-1}. The catalyst has a high activity resistance in both media.
3. The Pd-Al-Si/rGO catalyst was successfully synthesized, highly active in the ethanol oxidation, in an alkaline medium. Accordingly, the activity of the Pd-Al-Si/rGO catalyst was about 45.7% higher than the non-modified catalyst, Pd/rGO. On the same catalyst system, the reducing agent $NaBH_4$ was more effective than the reducing agent EG, shown at the particle size Pd about three times smaller, the catalytic activity increased by about 36.8%. In particular, it was found that the presence of Na in the catalyst component was reduced by $NaBH_4$.
4. The effect of denaturing agent Na on the activity and activity durability of the Pd/rGO catalyst was studied. In particular, the Pd-Al-Si-Na/rGO catalyst, reduced by $NaBH_4$, had an I_F value of 16138 mA mg_{Pd}^{-1}, the highest among published work on catalysis on a Pd basis. Besides, Na significantly increased the activity durability and anti-poisoning ability of the Pd / rGO catalyst, in the ethanol oxidation expressed in the I_F 500^{th} value decreased 32%.
5. The Pt-Al/rGO catalyst ink was successfully fabricated, used in DEFC. It has been determined that ethanol is the most suitable solvent for preparation CI-Pt-Al/rGO catalyst ink, expressed in ethanol oxidation, in both acidic and alkaline media with the highest value, corresponding to I_F of 1793 mA mg_{Pt}^{-1}, and 4751 mA mg_{Pt}^{-1}. On the other hand, no cracks on the electrode surface coated with the CI-EtOH(1/1) ink was observed. The maximum power density of PEM-DEFC and AEM-DEFC using CI-EtOH ink-coated anodes, reaching the highest value, respectively 19.10 mW cm^{-2} and 27.07 mW cm^{-2}.

6. Successfully fabricated the CI-Pd-Al-Si-Na/rGO catalyst ink with ethanol as solvent, applied like the anode in AEM-DEFC. No cracks were observed on the electrode surface after coating the ink. Maximum power density of the cell reaches 43.0 mW cm^{-2}. The energy conversion efficiency was 7.89% after more than 7 working hours with stable potential about 0.5 to 0.6 V.

C- LIST OF PUBLISHED ARCTICLES

- **List of papers in national scientific journals**

1. Vũ Thị Thu Hà, **Nguyễn Minh Đăng**, Vũ Tuấn Anh, Trần Thị Liên, Nguyễn Quang Minh, "*Nghiên cứu độ ổn định hoạt tính oxi hóa điện hóa metanol và etanol của xúc tác Pt-AlOOH-SiO_2/rGO*," Tạp chí Xúc tác Hấp phụ, tập 5, số 4, trang 3–8, 2016.
2. Vũ Thị Thu Hà, Trần Thị Liên, **Nguyễn Minh Đăng**, Nguyễn Quang Minh, "*Tổng hợp xúc tác PtMe / rGO (Me = Ni , Co , Al , Al-Si) có hoạt tính điện hóa cao trong phản ứng oxi hóa etanol*," Tạp chí Khoa học Công nghệ Việt Nam, tập 16, số 5, trang 12–16, 2017.
3. Vũ Thị Thu Hà, **Nguyễn Minh Đăng**, Mai Ngọc Anh Tuấn, *"Ứng dụng xúc tác trên cơ sở Pd/rGO biến tính chế tạo điện cực anode trong pin nhiên liệu ethanol kiềm,"* Tạp chí Hóa học Ứng dụng, Số Chuyên đề 3, 2020.

- **List of papers in international scientific journals**

1. L. T. Tran, Q. M. Nguyen, **M. D. Nguyen**, H. N. Thi Le, T. T. Nguyen, and T. H. Thi Vu, "*Preparation and electrocatalytic characteristics of the Pt-based anode catalysts for ethanol oxidation in acid and alkaline media*," Int. J. Hydrogen Energy, vol. 43, no. 45, pp. 20563–20572, 2018.
2. T. H. T. Vu, M. H. Nguyen, and **M. D. Nguyen**, "*Synthesis of acidic heterogeneous catalysts with high stability based on graphene oxide/activated carbon composites for the esterification of lactic acid*," J. Chem., vol. 2019, , Article ID 7815697, 7 pages, 2019.

3. **M. D. Nguyen**, L. T. Tran, Q. M. Nguyen, T. T. Nguyen, and T. H. T. Vu, "*Enhancing Activity of Pd-Based/rGO Catalysts by Al-Si-Na Addition in Ethanol Electrooxidation in Alkaline Medium*," J. Chem., vol. 2019, Article ID 6842849, 13 pages, 2019.

- **Reports in scientific conferences**

1. T. H. T. Vu, **M. D. Nguyen**, L. T. Tran, T. T. Lam, Q. M. Nguyen, *"New results for direct alcohol fuel cell anode catalysts,"* Conference on Advanced Separation Science and Engineering – CASSE 2018, 18th – 21st December 2018, Hanoi, Vietnam.
2. T. H. T. Vu, **M. D. Nguyen**, L. T. Tran, T. T. Lam, Q. M. Nguyen, "*Enhancing Activity of Pd-based/rGO Catalysts by Al-Si-Na Addition in Ethanol Electrooxidation in AlkalineMedium*," The International Conference on Advanced Nanomaterials for Green Growth – ADMAT 2019, 5th – 7th April 2019, Hanoi, Vietnam.